Prediction of Shear Strength in SCS Panels with One-End Welded BP Shear Connector Using Numerical Modeling and Gene Expression Programming (GEP)

Mahdi Daliri [a],Hamed Ghovhani Arab [a,*],Mahmoud Miri [a] ,Seyed Hashem Khatibi[b]

[a] Civil Engineering Department, University of Sistan and Baluchestan, Zahedan, Iran

[b] Civil Engineering and Architectural Department, Faculty of Engineering, University of Torbat Heydarieh, Torbat Heydarieh, Iran

Abstract

Steel-concrete-steel (SCS) sandwich structures, comprising steel faceplates and a concrete core, are valued for their strength and durability. Among various shear connectors, one-end welded box-profile (BP) connectors have shown strong potential in resisting interfacial shear forces. However, no precise formula exists to estimate their shear strength, especially considering the overlap ratio. This study addresses this gap by developing a predictive model for the shear strength of these connectors. Using the Taguchi experimental design, 18 numerical models were created, varying connector width, thickness, concrete core strength, and overlap ratio. Finite element simulations, validated against experimental push-out tests, analyzed load-slip behavior and failure modes. A Gene Expression Programming (GEP) algorithm was applied to derive an equation linking shear strength to geometric and material properties.

The resulting equation demonstrated high accuracy, with a correlation coefficient (R) of 0.919 and lower error metrics compared to existing methods. By incorporating overlap ratio effects, this model provides engineers with a more precise tool for designing safer and more efficient SCS systems. The findings enhance the understanding of BP connector mechanics and offer a cost-effective approach for optimizing SCS structures in various structural applications.

Keywords: Steel-concrete-steel sandwich structure, BP connectors, Shear connectors**,** Push-out test, Shear resistance,SCS.

1. Introduction

Steel-concrete-steel (SCS) sandwich structures comprise a concrete core encased by two thin steel faceplates. Researchers initially proposed epoxy adhesive to join these components. However, they

* **Corresponding author. E-mail address: ghohani@eng.usb.ac.ir**

adopted mechanical shear connections due to the weakness of adhesive connections against interlayer shear. Over time, various mechanical connectors have been introduced, including angle shear connectors(Fig.1(a)) [1, 2], stud-bolt connectors(Fig.1(b)) [3-6], bi-steel connectors(Fig.1(c)) [7-9], J-hook connectors(Fig.1(d)) [10-12], separately corrugated strip (Fig.1(e)) [13-16] and box-profile (BP) connectors(Fig.1(f)) [17-19], Each connector type exhibits distinct geometric and behavioral characteristics.

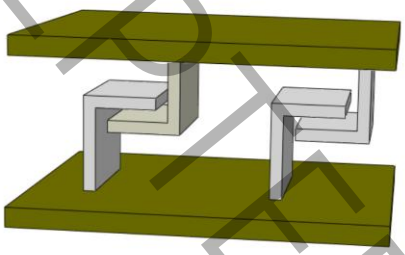

a)

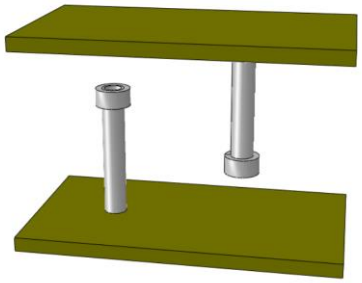

b)

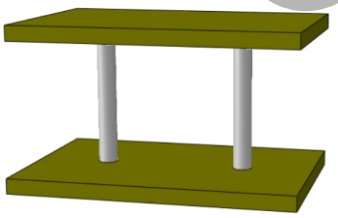

c)

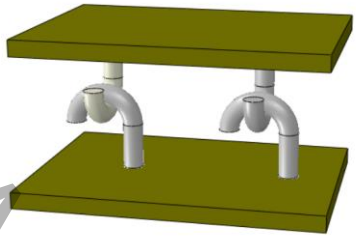

d)

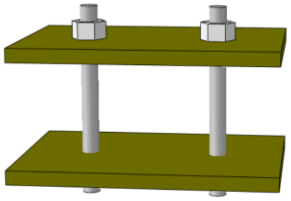

e)

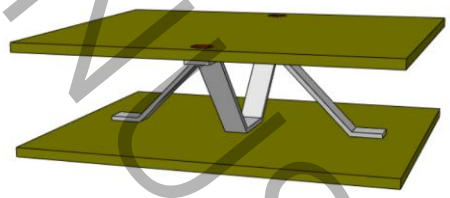

f)

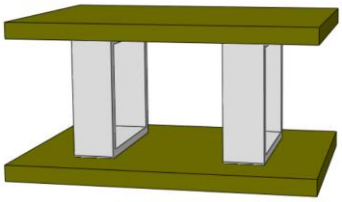

h)

Fig.1 . Shear connectors in SCS sandwiches, angle shear connectors(a),Double skin concrete system with stud shear connectors(b), bar shear connectors in Bi-steel system(c), J-hook shear connectors(d), separately corrugated strip shear connectors(SCSC)(e), Stud-bolt connectors in SCS (f), Box Profile Shear connectors(f).

In recent decades, this system has significantly advanced in the civil engineering field, with applications including immersed tube tunnels [20], bridges [21], offshore decks [22], oil tanks and shear walls [23], Below is a brief review of recent numerical and analytical studies on SCS structures.

In 2015, Jia-Bao Yan [24] modeled SCS beams with J-hook shear connectors under quasi-static loading. The study simplified J-hook connectors into bar elements and connected them using springs instead of explicitly modeling the hooks. The results indicated that the simulations accurately captured crack propagation and load-displacement curves.

In 2022, Chengfeng Xue et al. [25] welded the stud shear connectors to perforated faceplates, referred to as PBL connections. The researchers designed six SCS panels and conducted push-out tests. Subsequently, the specimens were modeled using finite element analysis (FEA) for validation. Additional simulations were performed to evaluate the effect of rebar thickness inside the perforations. The findings demonstrated that increasing the number of perforations and welded studs improved the shear behavior of the specimens, while thicker embedded rebars reduced concrete core damage and enhanced shear strength.

Yousefi et al. (2023) [26], conducted a numerical investigation into the flexural behavior of SCS sandwich slabs featuring studbolt shear connectors under quasi-static concentrated loads. The researchers validated the experimental specimens using the finite element method. Subsequently, the effects of parameters such as the thickness of steel faceplates, studbolt diameters, the thickness of the concrete core, and the center-to-center spacing of the studbolts were evaluated concerning failure modes and load-displacement curves. Finally, through full-factorial experimental design, several numerical models were developed to predict the ultimate strength of the slabs, and a simplified formula was proposed for estimating the ultimate strength of SCS slabs with studbolt shear connectors using Gene Expression Programming (GEP).

While advantageous in certain aspects, each of the shear connectors proposed by researchers also exhibits specific drawbacks. For instance, stud shear connectors lack the structural integrity to prevent separation between the steel faceplates after impact and crack formation. On the other hand, two-end stud connectors, although highly resistant to separation, face limitations in thickness due to the need for friction welding and are associated with high costs. J-hook connectors were introduced to address these challenges and eliminate thickness restrictions. However, implementing J-hook connectors in large-scale applications, ensuring all hooks interlock effectively, remains highly challenging.

In 2022, Khatibi et al. [17] introduced a novel shear connector called the Box-Profile (BP). This connector is easy to implement and, due to the continuity of the steel faceplates, does not experience a significant reduction in interfacial shear strength following crack formation in the concrete core, similar to stud connectors. Additionally, because the BP connectors are roll-formed, they do not require bending operations as seen with discrete strip or J-hook connectors, simplifying their implementation. Furthermore, the larger weld areas of BP connectors provide greater resistance to separation.

To investigate the interfacial shear strength of BP connectors, Khatibi et al. (2022) [17] performed push-out tests on BP specimens. Eight SCS panels with BP connectors were subjected to push-out tests, and the effects of geometric parameters, such as concrete core thickness, connector thickness and width, and BP placement, on interfacial shear strength were examined. However, the limited number of specimens prevented the development of a reliable formula for predicting the shear strength of the samples.

In another study, Khatibi et al. examined the flexural behavior of beams with BP connectors [18]. Nine beam specimens underwent three-point bending tests, and the influence of connector thickness, width, and concrete core thickness was analyzed. The effects of concrete core strength and BP connector arrangement on the flexural behavior were also investigated using finite element analysis.

As the construction of SCS beams with BP shear connectors imposes limitations on thickness, Daliri et al. (2025) [19] proposed a modified BP shear connector design featuring one-end welded and one-end embedded in the concrete core. They also studied the effect of overlap ratios for these connectors. The results indicated that the overlap ratio of BP connectors significantly influences

the shear strength of SCS specimens, but the limited number of specimens precluded the proposal of a predictive formula for this ratios.

Despite recent advancements, there remains a significant gap in understanding the shear behavior of BP shear connectors welded at one end. Previous studies have primarily focused on other types of shear connectors, and the overlapping behavior of this specific type has not been comprehensively investigated. The aim of this study is to bridge this gap and provide a comprehensive relationship for estimating the interlayer shear resistance of SCS structures with BP shear connectors welded at one end, considering different overlap ratios.

3-Ditales of Spicemens

Fig. 2 depicts the fabrication stages of the specimens. Initially, the BP connectors were welded to the steel faceplate using fillet welds at one end (Fig. (2-a)). After positioning the second faceplate, partial penetration welds were applied to secure the assembly (Fig.(2-b)). Finally, the specimens were cast and cured (Fig.(2-c)). The details of the experimental specimens are listed in Table 1. As shown in Fig 2, the parameters bc, tc ,h_{con}, hc ,hh represent the connector width, connector thickness, concrete core thickness, connector height, and the overlap ratio of the BP shear connectors, respectively.

To evaluate the shear resistance of shear connectors in SCS structures, push-out tests, as shown in Fig. 3, were used. Daliri et al. [19] conducted experiments to assess the effect of BP shear connector overlaps on shear resistance, considering laboratory constraints. The specimens listed in Table 1 were constructed and tested.

The steel properties of the tested specimens, as per the referenced article [17], are provided in Table 2. Additionally, all specimens were constructed using concrete with a compressive strength of 39 MPa.

Table 1. Specifications of Sample Dimensions for Testing Push-out [19]

Spicemen	h_{con} (mm)	bc (mm)	tc (mm)	hh (h_c/h_{con})
BP100-20	100	20	4	1
BP120-20	120	20	4	0.66
BP140-20	140	20	4	0.428
BP160-20	160	20	4	0.25
BP180-20	180	20	4	0.11
BP100-30	100	30	4	1
BP120-30	120	30	4	0.66
BP140-30	140	30	4	0.428
BP160-30	160	30	4	0.25
BP180-30	180	30	4	0.11
BP100-40	100	40	4	1
BP120-40	120	40	4	0.66
BP140-40	140	40	4	0.428
BP160-40	160	40	4	0.25
BP180-40	180	40	4	0.11

*Note: h_c=100 mm

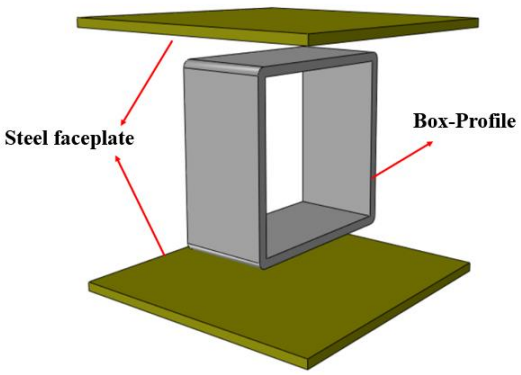

a) Components

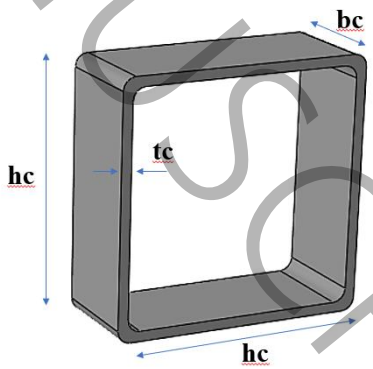

b) BP Shear Connector Details

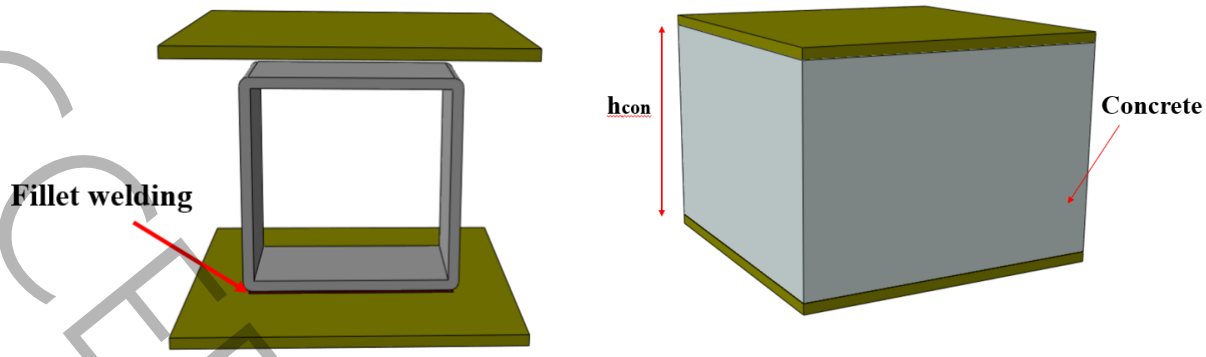

c) BP Shear Connector Attachment to the Steel Face

d) Concrete Pouring

Fig.2 . depicts the fabrication stages of the specimens

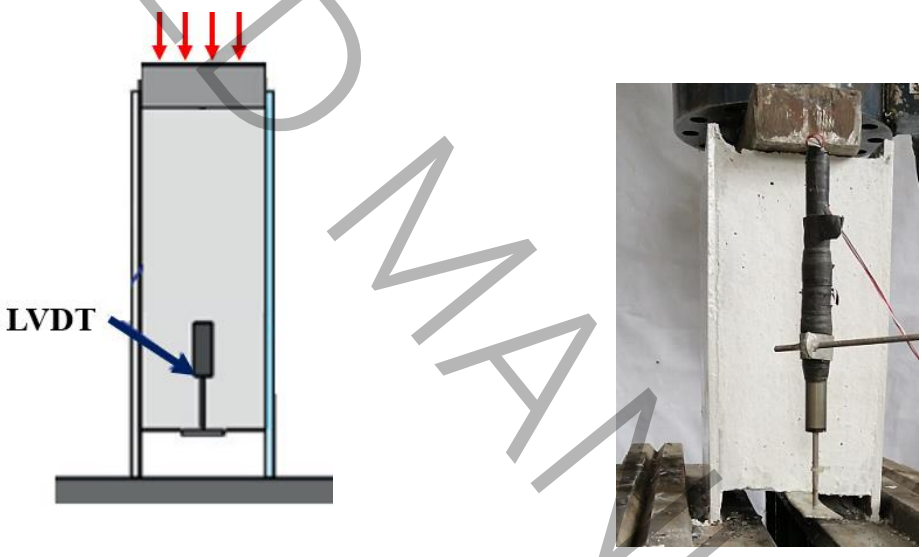

Fig. 3. Push-out test setup [17].

Table 2 . Properties of Steel Material[17].

Thickness	Yield Stress (MPa)	Ultimate Stress (MPa)	Strain at Ultimate Stress	Modulus of Elasticity (GPa)
4	250	380	0.3	207
Profile 100×100×4	285	495	0.23	202

3. Finite Element Model

In this section, the experimental specimens were modeled using the finite element software ABAQUS with an Explicit solver.

3.1. Modeling of Steel Materials

The isotropic strain-hardening rule and an elastoplastic model based on the von Mises yield criterion were used for modeling steel materials. The bilinear behavior of steel materials was defined using the reference study [17] and the data provided in Table 2.

3.2. Modeling of Concrete Materials

The concrete core was modeled using the Concrete Damaged Plasticity (CDP) model available in the ABAQUS material library [27]. The compressive behavior of concrete was predicted using the stress-strain equation specified by equations (1-3) [27].

(١)

$$\sigma_c = \frac{n f_c \varepsilon_c}{\varepsilon_0 (n - 1 + \left(\frac{\varepsilon_c}{\varepsilon_0}\right)^{nk})}$$

(٢)

$$n = 0.8 + \frac{f_c}{17}$$

(٣)

$$\begin{cases} k = 0.67 + (\frac{f_c}{62} & \varepsilon_c > \varepsilon_0 \\ k = 1 & \varepsilon_c \leq \varepsilon_0 \end{cases}$$

where f_c represents the cylinder compressive strength of the concrete sample, ε_0 represents strain corresponding to f_c, σc represents compressive stress, and $\varepsilon_c$represents compressive strain

Fig. 4 illustrates the compressive stress-strain diagram for concrete with a compressive strength of 39 MPa [19], derived using equation 1. It was used to model the concrete cores in SCS beams.

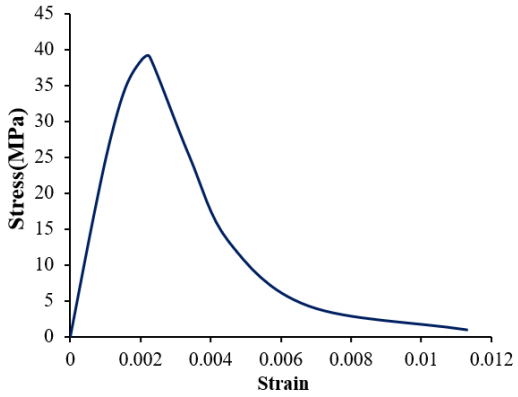

Fig. 4. Stress-Strain Curve Obtained for Normal Concrete

Huang et al. defined the damage parameters as expressed in equations (4) and (5) [26]

$$0 \le d_c = 1 - \frac{\sigma_c + n_c f_c}{E_c\left(\frac{n_c f_c}{E_C} + \varepsilon_c\right)} \le 1 \quad (4$$

$$0 \le d_t = 1 - \frac{\sigma_t + n_t f_t}{E_c\left(\frac{n_t f_t}{E_C} + \varepsilon_t\right)} \le 1 \quad (5$$

Parameters d_c and d_t represent compressive and tensile damage, respectively. Constants n_t and n_c denote compressive and tensile factors, with values ranging between 0 and 1. Additionally, f_t and E_C represent the concrete's tensile strength and elastic modulus. In this modeling, the tensile behavior of concrete was assumed linear up to its tensile strength, which, based on the reference study [19] as 3.1 MPa. Furthermore, the essential parameters were set as dilation angle (ψ) of 35°, flow potential eccentricity at 0.1, the biaxial-to-uniaxial compressive stress ratio ($f = f_{b0} / f_{c0}$) at 1.16, deviatoric stress shape parameter (k) at 0.667, and viscosity parameter at 0.001[18].

3. Boundary Conditions and Loading

In the push-out test modeling, as shown in Fig. 5, the supports were constrained against displacement in all three directions. Loading was applied quasi-statically to the rigid block. The interaction between concrete and steel faceplates and between BP connectors and the concrete core was simulated as Surface-to-Surface contact with Hard Contact formulation in the expected direction and Penalty Friction in the tangential direction. The friction coefficient for the shear connectors and steel faceplates in contact with the concrete was determined to be 0.15, obtained through trial and error.

Considering the complexity of the BP connectors' geometric model within the concrete core, quasi-static analysis with the Explicit solver and mass scaling was employed to reduce numerical analysis time. This approach involves virtually increasing the total mass of the model or a portion of it, which subsequently increases the stable time increment. When properly implemented, mass scaling reduces the computation time and maintains acceptable accuracy in the results.

In this study, the loading time was initially extended as much as possible to minimize acceleration. This increase in loading time significantly extended the analysis duration. Consequently, mass scaling was applied based on a predefined time increment for the entire model to reduce analysis time. The loading time and time step were carefully chosen to ensure the model was subjected to quasi-static loading.

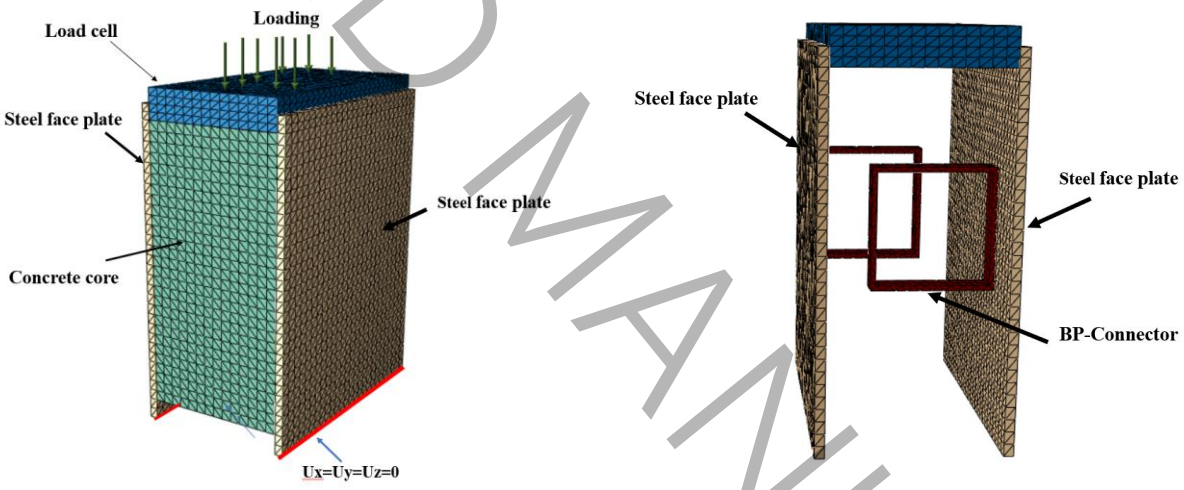

Fig. 5 .Finite Element Model of the Push-Out Test

3.4. Elements and Numerical Modeling

As shown in Fig. 6, the laboratory specimens comprised a load cell, steel faceplates, a concrete core, and BP connectors embedded in the concrete. The SCS beams were modeled using a 3D four-node continuum element (C3D4). As illustrated in Fig. 6, specimen N-1 was tested with three mesh sizes of 10 mm, 12 mm, and 15 mm, and the results were compared with experimental data. Ultimately, a 10 mm mesh size was selected based on the convergence trend of the graphs.

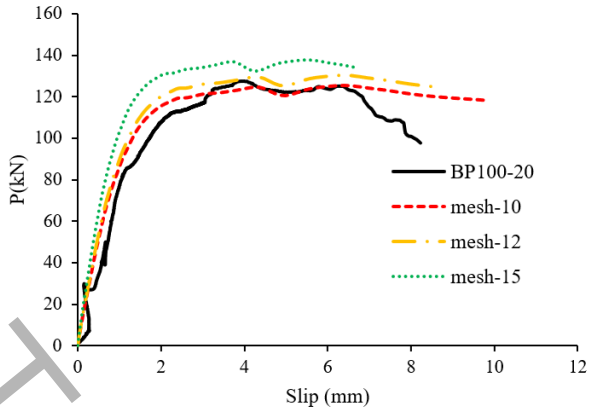

Fig. 6. Mesh Size Analysis for Modeling

3.5. Validation of Numerical Models

Given that mass scaling was employed for quasi-static loading in the explicit dynamic analysis, the ratio of external energy to internal energy ($\frac{Kinetic}{internalenergy}$) was monitored in all specimens to ensure it remained below 10%. Subsequently, the load-displacement curves and failure modes derived from the modeling were compared with experimental results.

3.6. Validation of Load-Displacement Curves and Failure Modes

Fig. 7 compares the load-displacement curves obtained from the modeling and experimental tests. It demonstrates that the finite element model successfully predicted the load-displacement behavior of SCS specimens with BP connectors. The slight discrepancy between the experimental and modeling results can be attributed to the simplification of steel material properties as bilinear. Table 3 compares the ultimate strength values derived from the finite element analysis and experimental tests. According to Table 3, the mean and coefficient of variation of the ultimate strength obtained from the finite element analysis compared to the experiments were 0.992 and 0.004, respectively. Therefore, the ultimate strength obtained from the experiments showed an acceptable correlation with the numerical results.

Furthermore, Fig. 8 illustrates that the finite element model provided reasonable predictions regarding the deformation of BP connectors after failure and the specimens' failure mechanism.

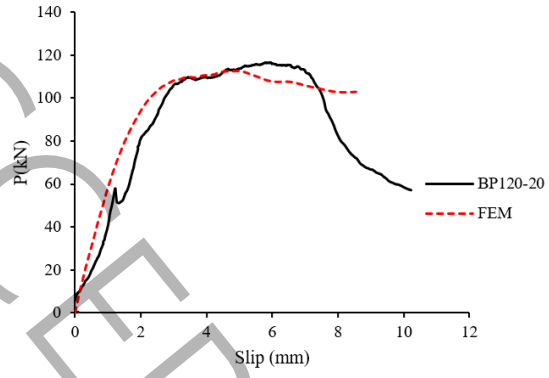

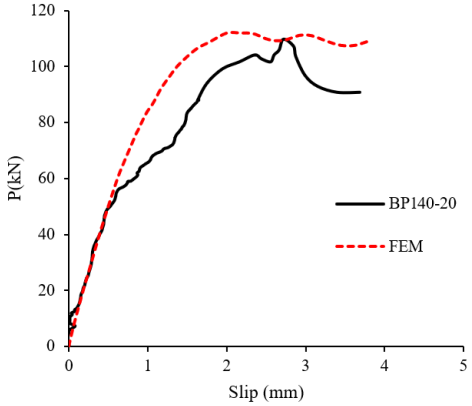

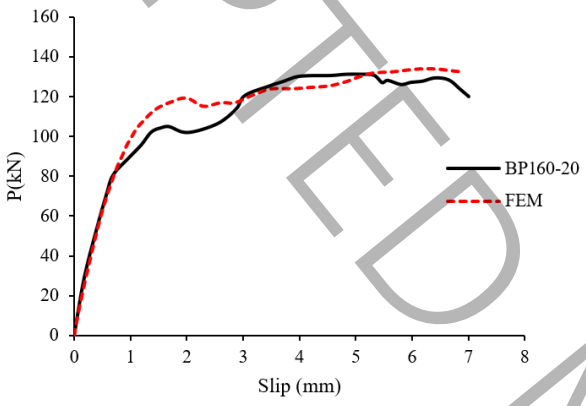

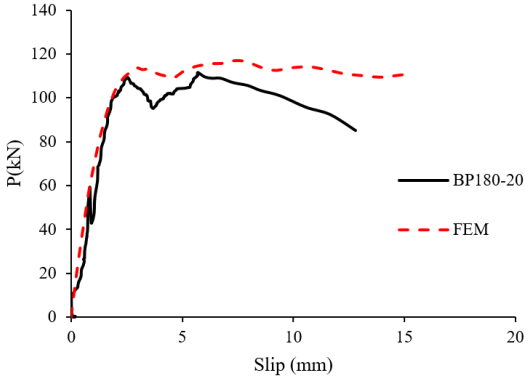

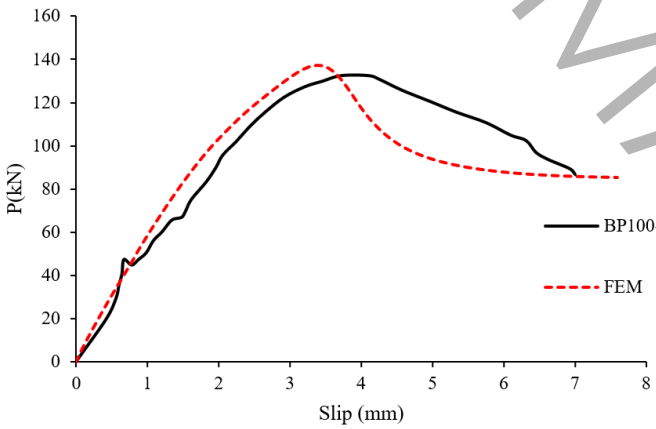

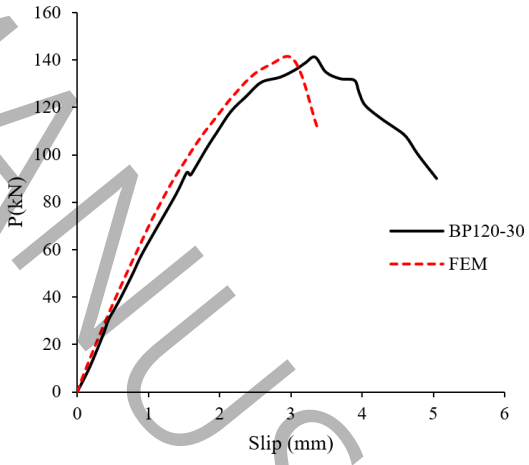

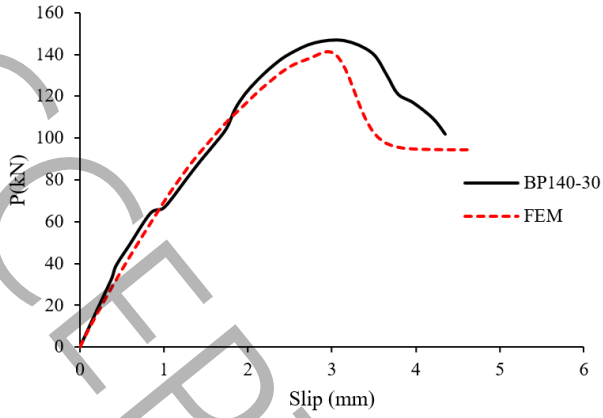

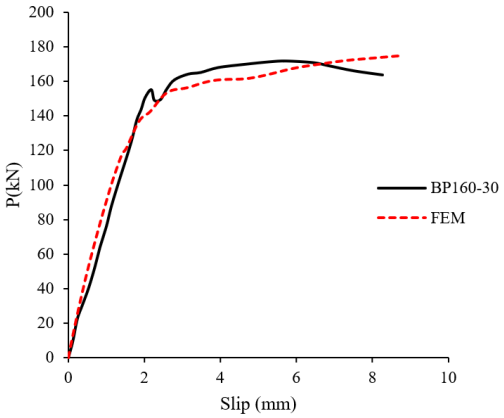

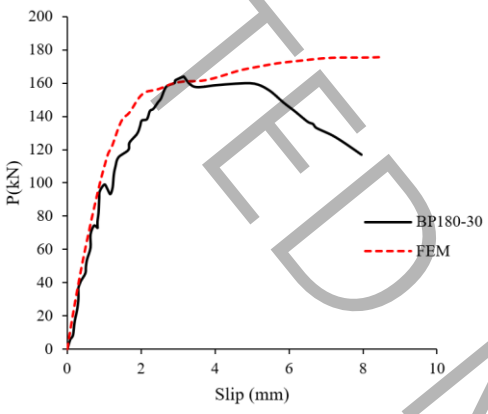

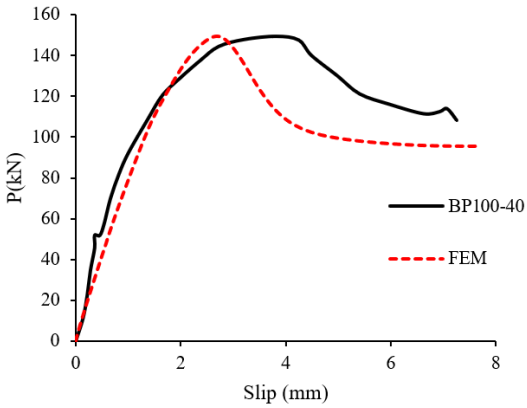

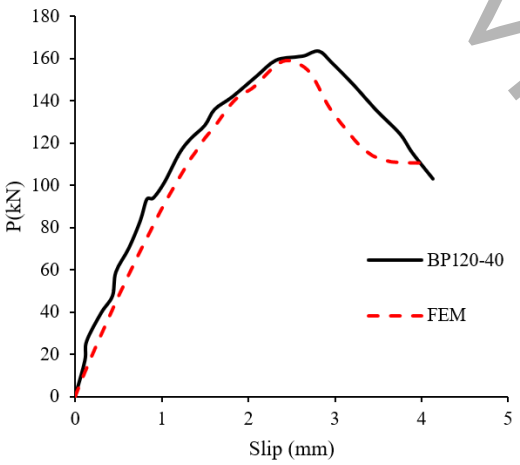

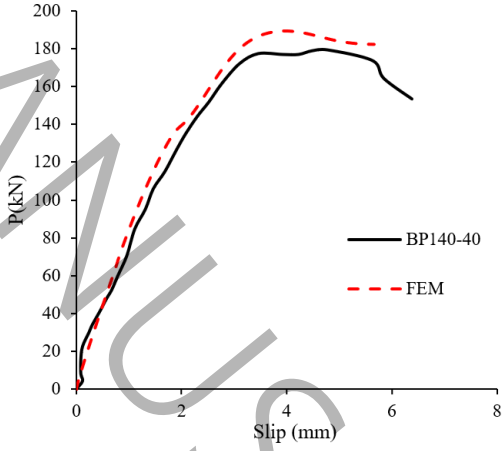

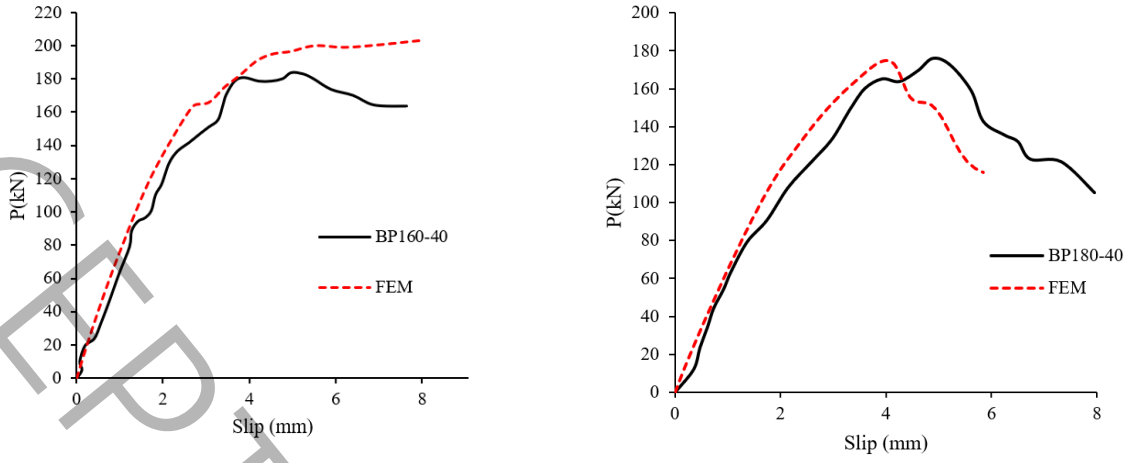

Fig. 7. Load-Slip Curve of Finite Element and Experimental Results for BP Specimens.

Table 3. Comparison of Ultimate Strength Obtained from Modeling and Experimentation

Specimen	F_{ut} (kN)	F_{un} (kN)	$\frac{F_{un}}{F_{ut}}$
BP100-20	127.65	125.35	0.982
BP120-20	130	112.65	0.866
BP140-20	109.83	96.20	0.878
BP160-20	131.21	133.88	1.02
BP180-20	111.56	116.96	1.046
BP100-30	132.33	121.59	0.919
BP120-30	141.3	141.22	0.999
BP140-30	146.67	141.4	0.964
BP160-30	171.56	174.47	1.016
BP180-30	163.94	175.45	1.07
BP100-40	149.33	149.51	1.00
BP120-40	163.45	159.32	0.975
BP140-40	179.42	189.34	1.055
BP160-40	183.63	203.14	1.106
BP180-40	176.04	175	0.994
Average			0.992
C.O.V			0.004

*Explanations: F_{ut}: Ultimate strength obtained from the experiment F_{un}: Ultimate strength obtained from the modeling

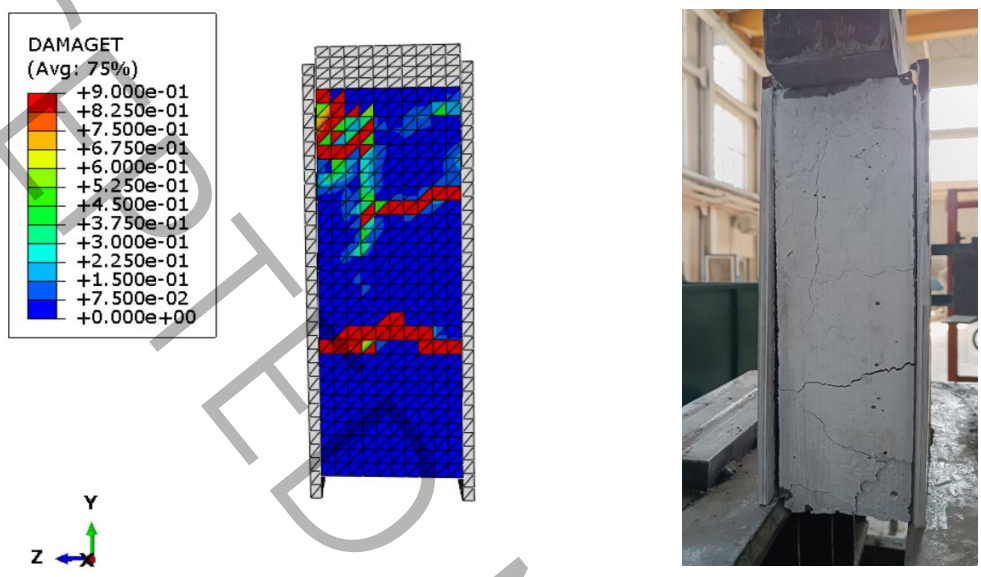

a) Failure of Specimen BP100-20

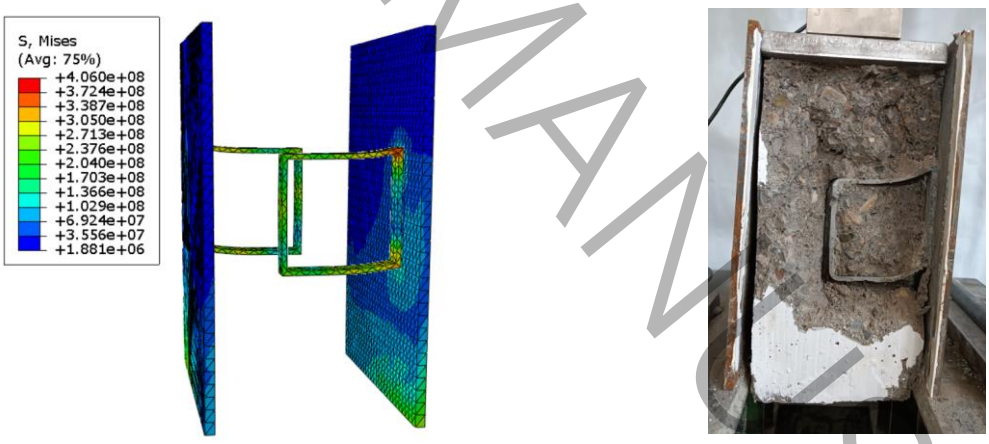

b) Deformation of BP Shear Connectors After Failure of Specimen BP160-20

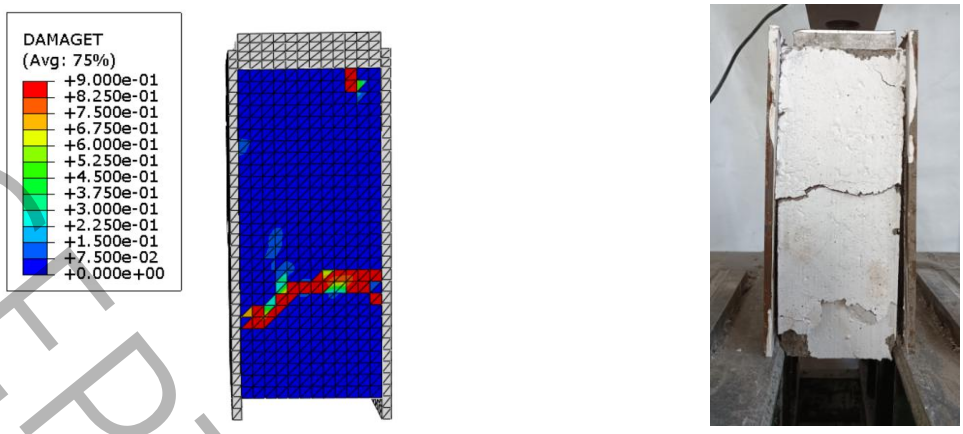

c) Failure of Specimen BP120-3

Fig 8. Failure of Experimental and FEM Specimens

4- Experimental Design

Several factors, such as the concrete core strength, connector thickness and width, and the concrete core thickness, can significantly influence the shear strength and behavior of SCS specimens. The simultaneous effects of these factors are notably complex and remain a subject of ongoing discussion. However, developing a reliable formula to estimate shear strength requires investigating the combined effects of these variables, necessitating extensive modeling, which is both time- and cost-intensive.

Due to laboratory constraints and the availability of materials, it was not possible to conduct experiments on various parameters. Therefore, the design of experiments method was not utilized for constructing the specimens. However, since there are no such limitations in modeling, the design of experiments approach was employed to comprehensively investigate the variables.

The Taguchi method of experimental design is an effective technique widely used in engineering analyses [3].

In fact, this method, by utilizing statistical and engineering concepts, has been introduced as a tool for improving product quality. Since the trial-and-error method is generally time-consuming and costly, it is necessary to achieve design objectives with a minimal number of experiments.

In this approach, deliberate changes are made to input variables to identify the extent of variations in the process response. Thus, by applying this method, controllable input factors can be systematically altered, and their effects on output parameters can be evaluated [28].

This method functions as an experimental design, employing orthogonal arrays to reduce the number of tests while minimizing the effects of uncontrollable variables. One of the most significant advantages of the Taguchi method is its ability to reduce testing time, thereby optimizing costs and enabling the identification of influential factors within a short period. This method organizes the primary parameters influencing a process's outcomes into different rows of an orthogonal array[17].

In this study, the Taguchi design of experiments method was employed to account for the interaction effects of geometric parameters and the strength of the concrete core. Finally, using the Gene Expression Programming (GEP) algorithm, a relationship was proposed that considers the failure modes of the concrete core and BP shear connectors.

Additionally, the proposed relationship was evaluated in terms of error parameters.

According to the study by Khatibi et al [17], when BP shear connectors are implemented with double-side welding, the shear strength of the specimens increases significantly. For this reason, in the tested specimens, failure modes were observed in both the shear connectors and the concrete core. However, when BP shear connectors are implemented with single-side welding [17], no failure was observed in the shear connectors.

It can be inferred that when BP shear connectors are implemented with single-side welding, the height of the connectors only serves to integrate the concrete and the steel plates, while the degree of overlap of the connectors (Fig. 9) plays a significant role in determining the shear strength. Therefore, the overlap ratio (hh) ($(\frac{l_c}{h_{con}})$ has been considered as an input parameter.

Finally, four input factors were considered as input variables: BP width (bc), BP thickness (tc), concrete core height (hcon), and compressive strength of the concrete core (fc), as shown in Table 4. Based on the designs obtained using the Taguchi experimental design method, 18 designs were created and modeled, as shown in Table 5.

It is worth mentioning that, to examine the effect of shear connector overlap, the height of the shear connectors (hc) was kept constant at 100 mm in all specimens.

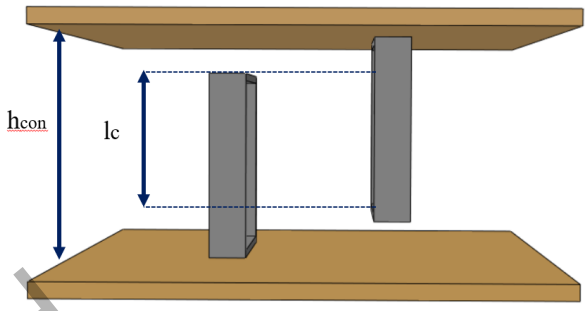

Fig.9. Sandwich system dimensions with One-end Welded Box-profile Shear Connectors

Table 4 - Input Parameters and Their Different Levels in the Taguchi Experimental Design

Parameters	Symbol	Levels					
		Level 1	Level 2	Level 3	Level 4	Level 5	Level 6
BP Width	b_c(mm)	20	30	40	-	-	-
BP Thickness	t_c(mm)	4	5	6	-	-	-
Concrete Core Thickness	h_{con}	190	180	160	140	120	100
Compressive Strength of Concrete Core	f_c(MPa)	30	40	50	-	-	-

Table 5. Geometric Specifications of Specimens and Corresponding Shear Strength for a Single BP Connector

Specimens	b_c(mm)	t_c(mm)	h_{con}	hh($\frac{l_c}{h_{con}}$)	f_c(MPa)	F_{uN} by FEA (kN)
test-1	20	6	120	0.66	40	72.63
test-2	30	4	120	0.66	50	75.21
test-3	30	4	100	1	30	63.16

test-4	40	5	100	1	40	86
test-5	20	6	100	1	50	80
test-6	20	6	180	0.11	50	75.27
test-7	30	5	160	0.25	30	81.74
test-8	30	6	160	0.25	40	100.64
test-9	40	5	160	0.25	50	108.25
test-10	40	6	140	0.428	30	112.44
test-11	20	4	140	0.428	40	57.4
test-12	30	5	140	0.428	50	84.71
test-13	40	5	120	0.66	30	69.93
test-14	20	4	190	0.052	30	52.5
test-15	20	5	190	0.052	40	74.55
test-16	40	6	190	0.052	50	118.65
test-17	30	4	180	0.11	30	59.22
test-18	40	5	180	0.11	40	82.18

5. Proposed Equation for Predicting the Interlayer Shear Strength of SCS Specimens Using Gene Expression Programming (GEP)

In 2001, Ferreira introduced Gene Expression Programming (GEP), a novel method combining Genetic Programming (GP) and Genetic Algorithm (GA). GEP employs linear chromosomes of fixed length, which resemble the tree structures used in Genetic Programming [29]. This method uses the provided dataset to generate a mathematical function [17]. Fundamentally, it operates on a genetic algorithm that selects data based on a fitness function and applies genetic modifications using one or more operators (genes). In GEP, the well-known roulette wheel selection method is used, and unlike GA and GP, multiple genetic operators can simultaneously propagate data. Replication ensures that several fit data points are carried forward from the current generation to the next, while mutation improves specific chromosomes randomly. Fig. 10 illustrates the GEP algorithm workflow in a flowchart [30].

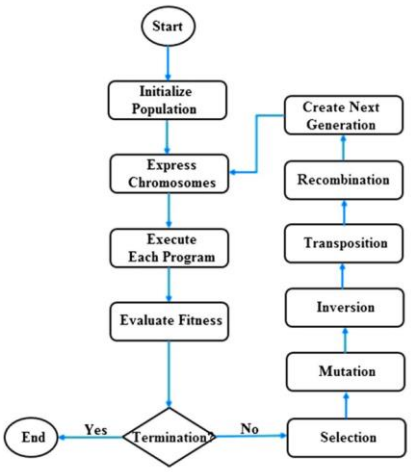

Fig.10 .Flowchart of the GEP Algorithm [31].

As shown in Table 5, the failure mode involving concrete failure was observed in both modeling and experiments. Equations related to concrete strength were derived using the genetic expression algorithm.

Thirteen numerical samples were used as training data (73%), and five were used as testing data (27%). The GEP algorithm parameters were set according to Table 6, with the fitness criterion minimizing the Root Mean Square Error (RMSE).

Table 6 - Parameters of the GEP Model

Parameter	Value
Function set	$\times, \div, \sqrt{\ }, \sqrt[3]{\ }$, Arctan
Head size	7
Chromosomes	50
Number of genes	2
Mutation rate	0.04
One-point recombination rate	0.3
Two-point recombination rate	0.3
Gene recombination rate	0.1
Gene transposition rate	0.1
Linking function	Multiplication

Since no failure was observed in the shear connectors in any of the experimental specimens, and due to practical limitations preventing the reduction of BP width beyond 20 mm, the proposed equation for estimating shear strength is based on concrete failure. However, if these limitations are not adhered to and the failure mode occurs in the steel, a minimum value for steel failure is considered.

The outputs obtained from the Gene Expression Programming (GEP) resulted in various equations for estimating the shear strength of BP connectors.

Ultimately, based on the minimum RMSE, Eq (6) was identified as the best equation derived from GEP.

$$P_u(kN) = \left(Arctan\left(\frac{2.58 \times h_{con}}{b_c \times hh^2}\right) \times \sqrt[3]{{t_c}^2 \times b_c \times f_c \times \sqrt{b_c}} \right) \times 1000 \leq 0.75 A_S F_u \quad (6$$

Fig. 11 compares the results predicted by GEP using Eq (6) with the training and experimental data.

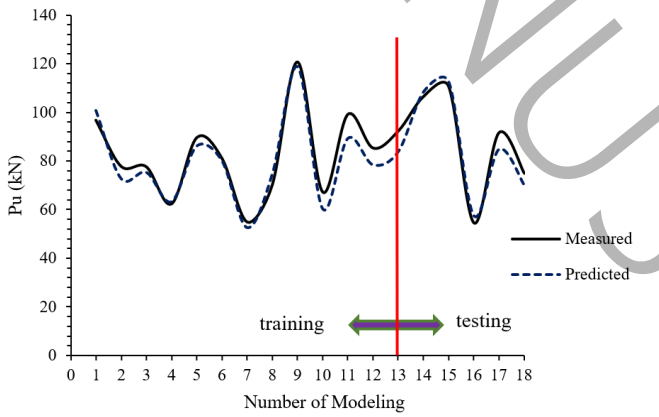

Fig. 11. Comparison of Predicted Data by the Proposed Equation with Modeling Data

6. Validation of the Proposed Equation

This section evaluates the shear strength derived from the proposed equation against the experimental results for BP connectors.

Fig. 12 compares the scatter of experimental results with the values obtained from the proposed equation. The range where the error is less than 10% is considered the "safe zone," while the remainder is deemed the "unsafe zone." Most ultimate strength values derived from the proposed equation fall within the safe zone. Subsequently, the results of the proposed equation are compared with those of established codes. Although the code equations are designed for other shear connectors, such as channel connectors and headed studs, the similarity of one-sided welded BP shear connectors to channel connectors justifies using shear strength equations for channel connectors from reliable codes.

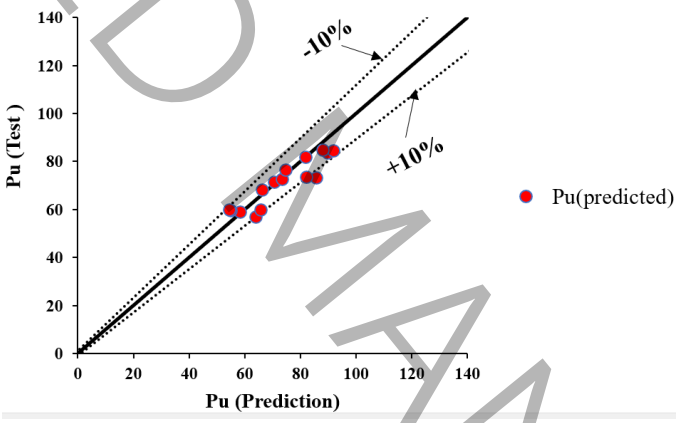

Fig. 12. Comparison Between the Proposed Equation and Experimental Results

Table 7 shows the existing code equations for calculating the shear strength of stud connectors. Considering that the cross-sectional area of stud connectors differs from that of BP shear connectors, the cross-sectional area of BP shear connectors has been calculated using Eq(7).

$$A_s = 2b_c t_c \quad (7$$

Table 7 . Shear Strength Equations for Connectors in Recognized Standards

Eurocode 4 (2004) [32]	$P_u = min\left(0.8f_u\frac{\pi d^2}{4\gamma_v}, 0.29\alpha d^2\frac{\sqrt{f_{ck}E_c}}{\gamma_v}\right)$ $\alpha = 1, \gamma_v = 1.25$
ANSI/AISC 360-10 [33]	$P_u = 0.5A_s\sqrt{f_{ck}E_c} \leq 0.75f_uA_s$
AASHTO Washington [34]	$P_u = 0.5A_s\emptyset\sqrt{f_{ck}E_c} \leq \emptyset f_uA_s$
GB 50017 [35]	$P_u = 0.43A_s\sqrt{f_{cp}E_c} < 0.7\gamma f_uA_s$

*__Explanations__: f_{ck}: Compressive strength of cylindrical specimens, f_{cp}: Compressive strength of prismatic concrete specimens, f_{cp}: Compressive strength of prismatic concrete specimens, f_u: Ultimate tensile strength of stud shear connectors, E_C: Secant modulus of elasticity of concrete, $\emptyset$: Strength reduction factor = 0.85, γ: Ratio of minimum tensile strength to yield strength of stud shear connectors

Table 8 compares the shear strength values of 15 experimental samples with those derived from the proposed and existing code equations. According to the results, the mean and coefficient of variation of the experimental-to-predicted shear strength ratio for the proposed equation are 1.030 and 0.0053, respectively, indicating better performance than the other equations.

Table 8. Comparison of Experimental and Modeling Results with Code Equations and the Proposed Equation

Spicemens	Pu_{exp}	Proposed Equation		Eurocode4		ANSI/AISC		AASHTO		GB50017	
		Pu_{pre} (kN)	$\frac{Pu_{exp}}{Pu_{pre}}$	Pu_{Euro} (kN)	$\frac{Pu_{exp}}{Pu_{Euro}}$	Pu_{AN} (kN)	$\frac{Pu_{exp}}{Pu_{AN}}$	Pu_{AASHTO} (kN)	$\frac{Pu_{exp}}{Pu_{AA}}$	Pu_{GB} (kN)	$\frac{Pu_{exp}}{Pu_{GB}}$
BP100-20	63.82	57.08	1.12	39.84	1.60	59.40	1.07	67.32	0.95	55.44	1.15
BP120-20	58.18	58.96	0.99	39.84	1.46	59.40	0.98	67.32	0.86	55.44	1.05
BP140-20	54.91	59.64	0.92	39.84	1.38	59.40	0.92	67.32	0.82	55.44	0.99
BP160-20	65.6	59.91	1.10	39.84	1.65	59.40	1.1	67.32	0.97	55.44	1.18
BP180-20	54.52	60.01	0.91	39.84	1.37	59.40	0.92	67.32	0.81	55.44	0.98
BP100-30	66.16	68.12	0.97	59.76	1.11	89.10	0.74	100.98	0.66	83.16	0.80
BP120-30	70.65	71.55	0.99	59.76	1.18	89.10	0.79	100.98	0.70	83.16	0.85
BP140-30	73.33	72.81	1.01	59.76	1.23	89.10	0.82	100.98	0.73	83.16	0.88
BP160-30	85.75	73.31	1.17	59.76	1.43	89.10	0.96	100.98	0.85	83.16	1.03
BP180-30	81.95	73.48	1.12	59.76	1.37	89.10	0.92	100.98	0.81	83.16	0.99

BP100-40	74.65	76.61	0.97	79.68	0.94	118.80	0.63	134.64	0.55	110.88	0.67
BP120-40	81.72	81.87	1.00	79.68	1.03	118.80	0.69	134.64	0.61	110.88	0.74
BP140-40	89.71	83.80	1.07	79.68	1.13	118.80	0.76	134.64	0.67	110.88	0.81
BP160-40	91.8	84.57	1.09	79.68	1.15	118.80	0.77	134.64	0.68	110.88	0.83
BP180-40	88	84.84	1.04	79.68	1.10	118.80	0.74	134.64	0.65	110.88	0.79
Ave			1.030		1.27		0.86		0.75		0.92
C.O.V			0.0053		0.0309		0.0343		0.0184		0.0219

*C.O.V: coefficient of variance;Pu_{pre} : prediction shear strength ; Pu_{exp}: experimental shear strength of BP, Pu_{euro}: prediction by Eurocode4; Pu_{An} prediction by ANSI/AISC; Pu_{AA}: prediction by AASHTO; Pu_{GB} prediction by GB50017

To ensure the proposed equation's reliability, it was evaluated using the correlation coefficient (R)[1], which indicates the linear relationship between two variables, and two error metrics: the Root-Mean-Square Error (RMSE)[2] and the Mean Absolute Percentage Error (MAPE)[3], as defined in Eq (7) through (9).

$$R = \frac{\sum_{i=1}^{n}(V_{exp} - V_{pre})(V_{pre} - \bar{V}_{exp})}{\sqrt{\sum_{i=1}^{n}(V_{exp} - \bar{V}_{exp})^2}\sqrt{\sum_{i=1}^{n}(V_{pre} - \bar{V}_{pre})^2}} \quad (7$$

$$RMSE = \frac{\sqrt{\sum_{i=1}^{n}(V_{exp} - V_{pre})^2}}{n} \quad (8$$

$$MAPE = \frac{\sum_{i=1}^{n}\left|\left(\frac{V_{exp} - V_{pre}}{V_{exp}}\right)\right|}{n} \times 100 \quad (9$$

In these equations, the parameters V_{exp}, V_{pri}, $\overline{V}_{exp}$, $\overline{V}_{pre}$, and n represent the experimental shear strength, predicted shear strength, mean experimental shear strength, mean predicted shear strength, and the total number of samples, respectively. The ideal R, RMSE, and MAPE values are 1, 0, and 0, respectively.

Table 9 evaluates the proposed equation using these error metrics. The efficiency of the shear strength prediction equations was assessed based on the correlation coefficient (R). In contrast, the prediction errors were evaluated using the Mean Absolute Percentage Error (MAPE) and the Root-

[1] Correlation coefficient

[2] Root-Mean-Square Error

[3] Mean Absolute Percentage Error

Mean-Square Error (RMSE). According to the results, Eq (6) exhibited the highest correlation coefficient (0.919), the lowest MAPE (6%), and the lowest RMSE (1.437) compared to the other equations.

These findings suggest that the proposed equation performs relatively well in estimating the shear strength of BP shear connectors.

Table 9. Comparison of Error Measurement Parameters

Equation	**Index**		
	R	**RMSE**	**MAPE(%)**
prediction by Eq(6)	0.919	1.435	5.99
Eurocode4	0.703	4.15	20.45
ANSI/AISC	0.689	5.629	22.13
AASHTO	0.581	8.521	35.93
GB50017	0.757	8.521	19.36

9. Conclusion

In this study, the Profile Box (BP) shear connector, which was implemented with single-side welding by Daliri et al.[19], was evaluated. First, 15 push-out test samples were modeled and validated against the experimental results regarding failure mode and load-slip curve. Since no relationship has been proposed to predict the shear strength of one-sided welded BP shear connectors, and given the differences in shear connector shapes, code equations cannot be relied upon; this research proposes a relationship with acceptable accuracy for estimating the shear strength of SCS beams with BP shear connectors.

Initially, using Taguchi's experimental design and considering the interactions of parameters such as thickness, width, and ultimate strength of BP shear connectors and the height and compressive strength of the concrete core, 18 samples were designed and modeled. Subsequently, the following relationship was proposed using the Genetic Expression Programming (GEP) algorithm.

$$P_u(kN) = \left(Arctan\left(\frac{2.58 \times h_{con}}{b_c \times hh^2}\right) \times \sqrt[3]{{t_c}^2 \times b_c \times f_c \times \sqrt{b_c}}\ \right) \times 1000$$

Since every proposed relationship requires performance and error evaluation tests, the values obtained from the proposed equation were compared with experimental results. To demonstrate the linear relationship, the correlation coefficient (R) was used, and to assess the error magnitude, the Mean Absolute Percentage Error (MAPE) and Root-Mean-Square Error (RMSE) criteria were applied. Based on the results, the proposed relationship showed a correlation coefficient 0.919, the lowest MAPE of 5.99%, and the smallest RMSE of 1.437 compared to code equations. Given the results of performance and error evaluations, the proposed equation performs relatively well in estimating the shear strength of BP shear connectors.

References

[1] R.S.N. Shariati M, Shariati A, Kueh ABH, Comparative performance of channel and angle shear connectors in high strength concrete composites: An experimental study, Constr Build Mater, (92) (2016) 120:382.

[2] N. Malek, Steel-concrete sandwich members without shear reinforcement, Transactions of Japan Concrete Institute (23) (1993) p27-34.

[3] Z. Huang, J.R. Liew, Nonlinear finite element modelling and parametric study of curved steel–concrete–steel double skin composite panels infilled with ultra-lightweight cement composite, Construction and Building Materials, 95 (2015) 922-938.

[4] Y. Lin, J. Yan, Y. Wang, F. Fan, C. Zou, Shear failure mechanisms of SCS sandwich beams considering bond-slip between steel plates and concrete, Engineering Structures, 181 (2019) 458-475.

[5] Y. Lin, J. Yan, Z. Cao, X. Zeng, F. Fan, C. Zou, Ultimate strength behaviour of S-UHPC-S and SCS sandwich beams under shear loads, Journal of Constructional Steel Research, 149 (2018) 195-206.

[6] Z. Wang, J. Yan, Y. Lin, F. Fan, Y. Yang, Mechanical properties of steel-UHPC-steel slabs under concentrated loads considering composite action, Engineering Structures, 222 (2020) 111095.

[7] M. Xie, N. Foundoukos, J. Chapman, Experimental and numerical investigation on the shear behaviour of friction-welded bar–plate connections embedded in concrete, Journal of Constructional Steel Research, 61(5) (2005) 625-649.

[8] N. Anandavalli, J. Rajasankar, A. Prakash, B. Sivaprasad, Static response of steel-concrete-steel sandwich beam with bi-directionally inclined connectors, American Journal of Civil Engineering and Architecture, 1(1) (2013) 15-20.

[9] Y.-T. Guo, M.-X. Tao, X. Nie, S.-Y. Qiu, L. Tang, J.-S. Fan, Experimental and theoretical studies on the shear resistance of steel–concrete–steel composite structures with bidirectional steel webs, Journal of Structural Engineering, 144(10) (2018) 04018172.

[10] J.-B. Yan, Y.-Y. Yan, T. Wang, Z.-X. Li, Seismic behaviours of SCS sandwich shear walls using J-hook connectors, Thin-Walled Structures, 144 (2019) 106308.

[11] W. Zhang, Z. Huang, Z. Fu, X. Qian, Y. Zhou, L. Sui, Shear resistance behavior of partially composite Steel-Concrete-Steel sandwich beams considering bond-slip effect, Engineering Structures, 210 (2020) 110394.

[12] J.-B. Yan, H. Hu, T. Wang, Flexural behaviours of steel-UHPC-steel sandwich beams with J-hook connectors, Journal of Constructional Steel Research, 169 (2020) 106014.

[13] H. Roshani, M. Yousefi, N. Gharaei-Moghaddam, S.H. Khatibi, Flexural performance of steel-concrete-steel sandwich beams with lightweight fiber-reinforced concrete and corrugated-strip

connectors: Experimental tests and numerical modeling, Case Studies in Construction Materials, 18 (2023) e02138.
[14] M. Yousefi, S.H. Khatibi, Experimental and numerical study of the flexural behavior of steel–concrete-steel sandwich beams with corrugated-strip shear connectors, Engineering Structures, 242 (2021) 112559.
[15] M. Yousefi, M. Ghalehnovi, Push-out test on the one end welded corrugated-strip connectors in steel-concrete-steel sandwich structure, Steel Compos. Struct, 24(1) (2017) 23-35.
[16] M. Yousefi, M. Ghalehnovi, Finite element model for interlayer behavior of double skin steel-concrete-steel sandwich structure with corrugated-strip shear connectors, Steel Compos. Struct, 27(1) (2018) 123-133.
[17] S.H. Khatibi, H.G. Arab, M. Miri, Interlayer behavior investigation of box profile shear connectors in steel-concrete-steel sandwich structures, in: Structures, Elsevier, 2022, pp. 1031-1042.
[18] S.H. Khatibi, H.G. Arab, M. Miri, The behavior of steel-concrete-steel sandwich composite beams with box-profile shear connectors: Experimental and numerical, in: Structures, Elsevier, 2023, pp. 644-656.
[19] M. Daliri, H.G. Arab, M. Miri, S.H. Khatibi, Overlap effects of one-end welded box-profile shear connectors on interlayer shear behavior, in: Structures, Elsevier, 2025, pp. 107982.
[20] K.M.A. Sohel, J.R. Liew, C.G. Koh, Numerical modelling of lightweight Steel-Concrete-Steel sandwich composite beams subjected to impact, Thin-Walled Structures, 94 (2015) 135-146.
[21] X.-L. Gao, J.-Y. Wang, C. Bian, R.-C. Xiao, B. Ma, Experimental investigation on the behaviour of UHPC-steel composite slabs under hogging moment, Steel and Composite Structures, An International Journal, 42(6) (2022) 765-777.
[22] J.-B. Yan, J.R. Liew, M.-H. Zhang, K. Sohel, Experimental and analytical study on ultimate strength behavior of steel–concrete–steel sandwich composite beam structures, Materials and Structures, 48 (2015) 1523-1544.
[23] Z. Huang, J.R. Liew, Structural behaviour of steel–concrete–steel sandwich composite wall subjected to compression and end moment, Thin-Walled Structures, 98 (2016) 592-606.
[24] J.-B. Yan, Finite element analysis on steel–concrete–steel sandwich beams, Materials and Structures, 48(6) (2015) 1645-1667.
[25] C. Xue, Z. Fan, F. Wu, L. Liu, L. He, X. Cui, Research on the shear behaviour of composite shear connectors, Buildings, 12(10) (2022) 1726.
[26] M. Yousefi, M. Golmohammadi, S.H. Khatibi, M. Yaghoobi, Prediction of the punching load strength of SCS slabs with stud-bolt shear connectors using numerical modeling and GEP algorithm, Journal of Rehabilitation in Civil Engineering, 11(3) (2023) 68-87.
[27] A.S.U.s. Manual, Abaqus 6.11, **http://130.149**, 89(2080) (2012) v6.
[28] S. ZANJIRCHI, F. AZIZI, M. AMANI, DEVELOPING A MODEL FOR FORECASTING THE SUCCESS OF CONSTRUCTION PROJECTS INTEGRATION TAGUCHI (DOE) AND TAXONOMY, (2017).
[29] S.K. Khrais, Y. Lin, Wear mechanisms and tool performance of TiAlN PVD coated inserts during machining of AISI 4140 steel, Wear, 262(1-2) (2007) 64-69.
[30] F.S. Hoseinian, B. Rezai, E. Kowsari, Kinetic constant modeling of Zn (II) ion removal from synthetic wastewater by gene expression programing, Amirkabir Journal of Civil Engineering, 53(1) (2021) 261-272.
[31] D. Muñoz, Thesis Discovering unknown equations that describe large data sets using genetic programming techniques, Masters Thesis, Linköping Institute of Technology, 2005.
[32] D. Jahed Armaghani, R.S. Faradonbeh, E. Momeni, A. Fahimifar, M. Tahir, Performance prediction of tunnel boring machine through developing a gene expression programming equation, Engineering with Computers, 34(1) (2018) 129-141.
[33] C. Européen, Eurocode 2: Design of concrete structures—Part 1-1: General rules and rules for buildings, London: British Standard Institution, (2004) 37.

[34] A. Specification, Specification for structural steel buildings, ANSI/AISC, 36010 (2005).
[35] L. Aashto, Bridge design specifications, (1998).